HHS Public Access

Author manuscript

Laser Phys Lett. Author manuscript; available in PMC 2020 February 01.

Published in final edited form as:

Laser Phys Lett. 2019 February ; 16(2): . doi:10.1088/1612-202X/aaf89e.

Photoacoustic imaging of gold nanorods in the brain delivered via microbubble-assisted focused ultrasound: a tool for *in vivo* molecular neuroimaging

Robin K. Hartman[1,†], **Kristina A. Hallam**[1,2,†], **Eleanor M. Donnelly**[1], and **Stanislav Y. Emelianov**[1,2,*]

[1] School of Electrical and Computer Engineering, Georgia Institute of Technology, Atlanta, GA, USA

[2] Wallace H. Coulter Department of Biomedical Engineering, Georgia Institute of Technology and Emory University School of Medicine, Atlanta, GA, USA

Abstract

The protective barriers of the CNS present challenges during the treatment and monitoring of diseases. In particular, the blood brain barrier is a major hindrance to the delivery of imaging contrast agents and therapeutics to the brain. In this work, we use gas microbubble-assisted focused ultrasound to transiently open the blood brain barrier and locally deliver silica coated gold nanorods across the barrier. This particular nanoagent possesses a strong optical absorption which enables *in vivo* and *ex vivo* visualization of the delivered particles using ultrasound-guided photoacoustic imaging. The results of these studies demonstrate the potential of ultrasound-guided photoacoustics to image contrast agents delivered via microbubble-assisted focused ultrasound for longitudinal diagnostic imaging and for therapeutic monitoring of neurological diseases.

Keywords

Ultrasound and photoacoustic imaging; nanoparticles; blood brain barrier opening; focused ultrasound

1 Introduction

The brain and the CNS as a whole present a unique set of challenges which must be overcome in order to treat or diagnose diseases and disorders of the CNS. One of the major obstacles to delivering substances, diagnostic imaging contrast agents or pharmaceuticals, to the brain is the blood brain barrier (BBB). The BBB is a selectively permeable barrier formed by the tight junctions of endothelial cells within the brain vasculature. The purpose of the BBB is to prevent entry of pathogens and other harmful substances into the brain by separating the circulatory system from the brain tissue[1]. There are currently several clinically used methods for opening the BBB, but they are not without their pitfalls.

*corresponding author: stas@gatech.edu.
†equally contributing authors

Pharmaceutical induced disruption can result in widespread opening of the BBB, which greatly increases the risk of entry of undesired substances into the brain such as pathogens[2]. The BBB can also be opened surgically, but this carries all the inherent risk associated with neurosurgery. Focused ultrasound (FUS) mediated disruption of the BBB using gas microbubbles offers a minimally invasive, localized, and temporary approach to open the BBB[3,4]. In the presence of a FUS field, microbubbles oscillate and interact with the endothelial lining of the vasculature enabling stretching of tight junctions and increased uptake in mechanotransduction pathways[5,6]. Microbubble-assisted FUS opening of BBB has been studied and verified over the past 15 years and is a well-developed tool that can be used for localized delivery of agents to the brain[7].

Among the many uses of FUS BBB opening, it can be used to deliver contrast agents to specific regions of the brain for imaging purposes. There is a large attrition rate of promising preclinical results failing to be translated into significant positive clinical trial results, and one of the major reason for this, particularly in diseases of the CNS such as Alzheimer's Disease, is the lack of real time *in vivo* assessment of biomarker expression[8]. Monitoring these biomarkers in real time in animal models of disease could provide highly valuable information regarding the progression of the disease and the effectiveness and method of action of potential therapeutics. Indeed, advances in preclinical biomarker imaging may result in higher clinical translation success.

There are currently several imaging modalities capable of imaging biomarkers *in vivo* such as fluorescence microscopy and positron emission tomography (PET)[9,10]. Though all these methods are valuable and have their merit, they do have inherit pitfalls such as limited imaging depth, need for invasive craniotomy, cost, and concerns associated with radioactive compounds. Ultrasound and photoacoustic imaging (USPA), a dual imaging modality capable of high-resolution visualization of optical absorption at depths exceeding optical imaging methods and within the content of the ultrasound imaging, is well suited to overcome these problems. By delivering photoacoustically sensitive contrast via localized BBB opening into the brain, USPA imaging can simultaneously visualize anatomical, functional, and molecular properties of the brain at depths of a few centimeters, in real time, and without the need for a craniotomy[11,12].

Furthermore, because PA contrast agents have unique optical signatures related to their absorption spectra, they can be separated from any endogenous PA contrast[13]. By harnessing the capabilities of PA contrast agents, USPA imaging has the capability to provide longitudinal preclinical biomarker imaging which can help to further understand the progression of diseases like Alzheimer's. Currently, microbubble assisted FUS BBB opening has been used to deliver gold nanorods for photoacoustic microcopy to monitor BBB behavior in response to FUS opening[14]. In this work, we examine and confirm noninvasive USPA imaging of locally FUS delivered silica coated gold nanorods (Si-AuNRs) on a whole brain scale. Thus, we are able to demonstrate selective delivery and *in vivo* imaging of PA contrast in the brain.

2 Materials and Methods

All chemicals and reagents were obtained from Sigma-Aldrich (St. Louis, MO) unless otherwise stated.

2.1 Microbubbles and contrast agents

Silica coated gold nanorods, with peak absorption wavelengths of 780 nm and 850 nm and a concentration of OD 100 were supplied courtesy of Nanohybrids, Inc (Austin, TX). Non-targeted Vevo MicroMarker microbubbles were supplied courtesy of Visualsonics, Inc (Toronto, CA). Evans Blue was used at a concentration of 3% W/V for all injections and microbubbles were used a concentration of 2×10^7 microbubbles/mL for all injections unless otherwise stated.

2.2 FUS transducers and system for BBB opening

Two types of single element transducers were used to open the BBB. For initial studies, a spherically-focused 2.25 MHz transducer (Valpey Fisher, Inc.) with a diameter of 1.5 inches and f-number of 1.3 was used. For positioning and delivery of the ultrasound field, a custom 3D printed, water filled coupling cone was made. For later studies, a 2 MHz transducer with 50 Ω matching circuit and polycarbonate coupling cone was used (H-148, SonicConcepts, Inc., Bothell, WA). For later studies, the 2 MHz single element transducer was used to improve the localization of the disruption footprint and reduce acoustic reflections from the bottom of the skull. The transducer had a 64 mm diameter, 31.5 mm radius of curvature, 20 mm central opening, and f-number of 1.00. In addition to the focused ultrasound transducer, the BBB opening system consisted of a function generator (Keysight Technologies, Inc.) to produce the source signal and a 50 dB RF amplifier (1040L, Electronics and Innovation, Inc.) to amplify the source signal prior to reaching the transducer. For precise positioning of the transducer, a three-dimensional positioning system consisting of three motorized translation stages (Newport, Inc.), a pulser/receiver (Olympus Co.), and a digital oscilloscope (Picoscope 3406D, Pico Technology) connected to a portable computer were used.

2.3 FUS BBB opening procedure

All animal studies were conducted under the protocol approved by the Institutional Animal Care and Use committee at Georgia Institute of Technology. *In vivo* animal studies consisted of FUS and microbubble BBB opening and *in vivo* imaging before and after the FUS opening procedure. Mice (C57BL/6) were anesthetized using a combination of 2% isoflurane and 0.6 L/min oxygen. Mice were positioned in a stereotax in the prone position, with a heating pad (Stoelting Co). Hair from the scalp was removed through shaving and depilatory cream. Proparacaine (0.5%, Henry Schein) was applied to the eyes, for pain relief. The transducer was positioned over the right parietal bone, such that the left side of the brain could serve as an internal control. The focal spot of the transducer was 2 mm laterally from the sagittal suture, and ~1mm below the surface of the skull. Axial position was measured using pulse-echo ultrasound. A co-injection of 50 μL of microbubbles (2×10^7 microbubbles/mL) and 50 μL AuNRs (Si-850 nm AuNRs in *ex vivo* studies and Si-780 nm AuNRS in *in vivo* studies) was injected retro-orbitally and sonication was initiated for 60

seconds. For both transducers, duty cycle was 10% and burst repetition frequency was 10 Hz. The pressure amplitude was set to achieve an *in vivo* mechanical index of 0.7, assuming 50% insertion loss from the skull[15]. After sonication, mice were allowed to recover from anesthesia for 4 hours before euthanasia. This 4 hour time point was chosen as this is likely the time when the BBB begins to close[1,16].

2.4 USPA imaging

Prior to commencing *in vivo* studies, we first completed preliminary studies *ex vivo* (n = 7 mice). *Ex vivo* studies were conducted prior to *in vivo* imaging to establish the appropriate USPA imaging protocol and to demonstrate the ability to spectroscopically distinguish the delivered particles from endogenous PA contrast. After mice underwent FUS BBB opening as outlined in section 2.3, mice were observed for 4 hours post-sonication, with no gross behavioral damage observed. Mice were then sacrificed via cardiac perfusion with PBS and 10% formalin, and heads were removed and post-fixed in formalin overnight. The excised tissue samples were visualized using a Vevo LAZR (VisualSonics, Inc.) imaging system. The imaging was performed without the skin, but with the skull intact, 24 hours after fixation. After imaging, the brain was carefully excised from the skull and imaged separately. Images with intact skulls were acquired with a 15 MHz or 21 MHz combined USPA imaging transducer (Vevo LZ201 and LZ250, respectively, VisualSonics, Inc.). Excised brains were imaged with a 40 MHz combined USPA imaging transducer (Vevo LZ550, VisualSonics, Inc.). All tissue samples were imaged on top of an 8% gelatin base in a container of degassed water. Whole brain US and spectroscopic PA image sets were acquired for each mouse with a distance step size of 0.1 mm both in the coronal and sagittal planes. PA images were acquired over 12 wavelengths (680 nm, 700–950 nm in 25 nm increments).

In vivo imaging was performed on animals sonicated using the 2 MHz focused ultrasound transducer (n = 5 mice). 3D spectroscopic coronal and sagittal USPA images were acquired, again over 12 wavelengths (680 nm, 700–950 nm in 25 nm increments). Four hours after sonication, mice were imaged using the 15 MHz transducer. Once the imaging session was complete, animals were euthanized as outlined above and *ex vivo* imaging was performed (section 2.3, 2.4).

2.5 Image processing

Real-time images were acquired and processed off-line using MATLAB (Mathworks, Inc.). In *ex vivo* experiments, expected sources of PA signal were the AuNRs and deoxygenated hemoglobin. As the tissues had been fixed in formalin for a minimum of 24 hours, it was assumed that oxygenated hemoglobin was no longer present. The absorption spectrum for the AuNRs was measured with a UV-VIS spectrometer (Evolution 220, Thermo Scientific). For deoxygenated hemoglobin, a published absorption spectrum was used for spectral unmixing[17]. PA signal from AuNRs was resolved using ratiometric analysis. Briefly, pixels were assigned to one of the two possible tissue components based on the ratio of PA signal intensity at two wavelengths: 850 nm and 680 nm, selected based on the absorption and PA spectra of AuNRs and deoxygenated hemoglobin. This method is applicable to cases where only two signal sources with significantly different absorption spectra are present.

In *in vivo* experiments, PA signal sources included AuNRs, deoxygenated hemoglobin, and oxygenated hemoglobin. Because there were three sources of contrast, a more advanced spectral unmixing algorithm was used to resolve the AuNRs[18,19]. In this approach, the signal at each pixel is assumed to result from multiple absorbers with known spectra and the contribution of each absorber to the signal was determined by fitting the PA signal at each pixel to the known spectra.

2.6 Histological Analysis

After completion of *ex vivo* imaging, all excised brains were cryopreserved in 30% sucrose in PBS and flash frozen for histological analysis. Frozen brains were cryosectioned to 20 and 40 μm thick coronal sections. Serial sections were stained for various markers of interest. Standard hematoxylin & eosin (H&E) staining was used to mark extravasated red blood cells and to visualize gross morphological changes. Two-photon microscopy microscope (LSM 710 NLO, Carl Zeiss AG) was used to confirm the presence of silica-coated gold nanorods. Prior to capturing photomicrographs, slides were soaked in PBS for 5 minutes. An excitation wavelength of 800 nm was used. An emission range between 460 and 700 nm was acquired.

3 Results

3.1 Characterization of USPA contrast agents

Prior to beginning animal studies, we first characterized the spectra of the contrast agents used. The absorption spectra for the contrast agents used in this study, along with endogenous absorbers, are shown in Figure 1. The spectrum for AuNRs where obtained via UV-Vis spectrometry. The spectra from both hemoglobin species was obtained from the literature[17]. The spectra shown for all potential sources of photoacoustic contrast were used in image analysis for the rest of the study. TEM images of the particles used are also shown in Figure 1(b).

3.2 Ex vivo imaging of AuNRs delivered to the brain using FUS and microbubbles

Figure 2 shows the results of our *ex vivo* imaging performed to optimize our approach prior to proceeding to *in vivo* studies. As seen in Figure 2(a), a localized PA signal is present in the left hemisphere of the brain, where FUS sonication occurred. The right contralateral side of the brain, which received no sonication and no observed signal, serves as an internal control. To examine the source of the produced PA signal, regions specified in Figure 2(a) were plotted over the wavelengths at which the PA signal was captured. Figure 2(b) shows a graph of the PA signal spectrum from both hemoglobin and Si-850 nm AuNRs obtained from the regions highlighted in 2(a). Using these trends and the ratiometric analysis described in the methods above, the images in Figure 2(c)–(d) were produced. In Figure 2(b), it can be seen that the region marked by a red oval follows a trend similar to the absorption spectra of the Si-850 nm AuNRs while the region marked by a blue oval follows a trend similar to the absorption spectra of deoxygenated hemoglobin. Figure 2(c) is the processed version of the image shown in 2(a), showing PA signal from Si-850 nm AuNRs in red heat map, and PA signal from hemoglobin in blue. Figure 2(d) shows a USPA image of the signal from Si-850 nm AuNRs as imaged through the intact skull, with skin removed. It

should be noted that these animals were perfused prior to imaging, and therefore any hemoglobin signal present is either due to hemorrhaging from sonication or due to incomplete perfusion. These results combined show that the Si-850 nm AuNRs were successfully delivered discretely and can be imaged via USPA through an intact skull and that the signal from the contrast agent can be separated from endogenous signal using ratiometric analysis.

3.3 In vivo imaging of AuNRs delivered to the brain using FUS and Microbubbles

Given the promising results of the *ex vivo* studies, *in vivo* studies were performed. In these experiments, FUS sonication occurred in the right side of the brain, with the left side acting as an internal control. *Ex vivo* imaging was preformed after the *in vivo* imaging to allow for confirmation of the PA signals observed *in vivo*. Figure 3 shows the PA signal captured in both *in vivo* (a,b,e,g) and *ex vivo* (b,d,f,h) imaging after a co-injection of microbubbles and Si-780 nm AuNRs and sonication. Spectral unmixing was performed for deoxyhemoglobin (Figure 3(c)–(d)), oxygenated hemoglobin (Figure 3(e)–(f)), and Si-780 nm AuNRs (Fiugre 3(g)–(h)) based on the spectra measured and reported in Figure 1. In both *in vivo* and *ex vivo* images, Si-780nm AuNR signal is present discreetly within the right hemisphere of the brain, while minimal hemoglobin signal is present in the area of Si-780 nm AuNR delivery. The differences in hemoglobin signal observed between the *in vivo* and *ex vivo* is due mainly to the removal of blood, by perfusion, prior to *ex vivo* imaging. Furthermore, difference in *in vivo* and *ex vivo* USPA imaging and PA signal comes from the use of different transducers (15 MHz and 40 MHz, respectively) as well as the physical acoustic barrier of the skull. However, these results show that USPA imaging is capable of imaging Si-AuNRs *in vivo* through the intact skulls, and that spectral unmixing can be used to adequately separate the signals from the different absorbers present.

3.4 Histological Analysis

In order to further investigate effects of FUS BBB opening on the brain, histological analysis was performed. Both the treated and untreated sides of the brain underwent standard H&E staining. H&E staining would highlight any hemorrhaging which may have occurred due to FUS BBB opening. Upon examination, both the treated and untreated regions are similar in morphology and staining, with no evidence of red blood cells with in the brain parenchyma, suggesting that no damage was incurred when sonication and delivery of Si-AuNRs was performed (Figure 4(a)). Delivery of Si-AuNRs was confirmed using two photon microscopy (Figure 4(b)). In the right hemisphere, signal from the AuNRs is discretely present as shown in the zoomed-in box to the right of the photomicrograph. Thus, in addition to USPA imaging, H&E staining and two photon microscopy demonstrate that Si-AuNRs are delivered to the brain without damage to the tissue.

4 Discussion

4.1 FUS delivery of AuNRs allows for in vivo USPA brain imaging

The results of these studies demonstrate the ability of FUS to deliver PA contrast agents to the brain. In both *ex* vivo and *in vivo* USPA imaging, AuNR signal is observed locally in the brain, where FUS is applied (Figures 2 and 3). Furthermore, signal from exogenous contrast

can be separated from that of endogeneous agents using ratiometric and spectral unmixing techniques. These techniques can be applied to *in vivo* USPA imaging, allowing for signal localization of delivered PA contrast agents. Furthermore, histology shows that particles have been successfully delivered to the tissue without damage, suggesting that FUS BBB opening and delivery of AuNRs is effective and safe (Figure 4). Overall, FUS delivery of PA contrast agents to the brain is significant, as it can allow for USPA imaging of selectively delivered particles. In addition, these particles can be imaged *in vivo*, and in real time, which further expands the applications of USPA imaging of the brain, especially in preclinical models.

4.2 Potential of in vivo USPA imaging for longitudinal monitoring of disease

Through the combination of FUS mediated opening and USPA imaging of delivered PA contrast agents, the ability to quantitatively and longitudinally measure PA signal in the brain is possible. This capability thus enables real time monitoring of brain function and how this may change with a disease state. One specific application of this particular method is for use in Alzheimer's disease. By functionalizing, via antibody conjugation or other targeting moiety, the PA contrast agent, SiAuNRs or others, can target plaques or tau proteins within the brain allowing the state of Alzheimer's disease to be evaluated *in vivo*[20,21]. As the disease progresses, PA signal can be monitored longitudinally to see how the distribution of the disease state changes within the tissue[21,22]. This data is of particular interest as current imaging techniques are unable to capture this information and provide insight into the disease progression on a molecular level in a way USPA imaging with PA contrast agents can[18,23]. Not only can PA contrast agents be used to monitor diseased tissue changes, but it also can be used to provide an improved understanding of the clearance system of the brain[22]. Thus, in the area of basic science, PA imaging has the potential to provide more insight into how the normal brain functions. Overall, this technique could enable an improved understanding of neurological function in both normal and diseased brain states.

4.3 Advantages of USPA imaging in the brain

The imaging techniques presented in this work possess advantages over other technologies currently used to monitor brain function. In particular, USPA imaging utilizing PA contrast agents capture both macroscopic and microscopic information about the brain. This range of signal is possible via the anatomical map provided by US imaging and the localized signal provided by the PA contrast. Optical imaging techniques like fluorescence microscopy, on the other hand, can only provide microscopic information, and although histology can provide both microscopic and macroscopic visualization, it can only be performed *ex vivo*[24]. PET requires a radiotracer, is bulky, and is expensive[25,26]. Although MRI has advantages over some of these other techniques, it too is expensive and can require additional imaging from modalities such as PET to generate both functional and morphological information[25]. By examining these disadvantages of other technologies, it is apparent that USPA imaging of selectively delivered PA contrast agents *in vivo* and in real time, has the potential to be the most effective option for longitudinal, preclinical imaging studies of neurological diseases.

4.4 Current Limitations

Although USPA imaging of FUS delivered contrast agents shows great promise, there are some aspects which must be improved before this technology can be employed robustly for preclinical longitudinal imaging. For example, PA signal of the delivered particles could be improved through better alignment of light delivery to the brain. Specifically, in the *in vivo* imaging sequences, where the lower frequency ultrasound transducers (i.e. 15 and 21 MHz) are used, the alignment of the USPA combined probe and the focal location of BBB opening (i.e. where the PA signal from the Si-AuNRs should be the greatest) is more difficult, as the position of the laser focus is shallower in depth than the location of the BBB opening. As a result, although some PA signal is captured and visualized (Figure 3), an external optical fiber aligned closer to the FUS opening may provide increased PA signal. Furthermore, there is no need to adjust the alignment of the ultrasound probe, as it is electronically focused. Another improvement is possible through application-specific PA contrast agent. Other particles, such as copper sulfide particles or liposomes encapsulated with dye, would be more biocompatible than AuNRs. Also, choosing a particle with a peak absorbing wavelength in the second optical window would reduce the signal produced via endogenous contrast such as deoxygenated and oxygenated hemoglobin. As seen in the Figures 2 and 3, both methods detected deoxygenated hemoglobin in *ex vivo* imaging procedures suggesting hemorrhaging and possible tissue damage. However, this phenomenon was not confirmed with H&E staining, which showed no gross tissue changes or leakage of red blood cells. As this deoxygenated hemoglobin was not apparent in histology, this signal could also be a result from the overlap of the deoxygenated hemoglobin and AuNR absorption. Therefore, care should be taken in PA contrast agent selection so that optimal spectral unmixing can be completed, improving signal localization in the tissue.

5 Conclusion

In conclusion, we have demonstrated the ability to successfully and locally deliver Si-AuNRs to the brain using FUS and to image this PA contrast agent using USPA imaging techniques. *In vivo* imaging of these discretely delivered particles across the BBB provides the basis for longitudinal UPSA imaging in the CNS. As this method has been demonstrated to be safe and effective, it has the potential to become a powerful tool for understanding the mechanisms of and evaluating the appropriate treatment choices for neurological disorders.

Acknowledgements

Funding for this study was provided by the National Institutes of Health (NIH) (NS102860).

References

1. Vykhodtseva N, McDannold N & Hynynen K Progress and problems in the application of focused ultrasound for blood-brain barrier disruption. Ultrasonics 48, 279–296, doi:10.1016/j.ultras.2008.04.004 (2008). [PubMed: 18511095]
2. Siegal T et al. In vivo assessment of the window of barrier opening after osmotic blood-brain barrier disruption in humans. J Neurosurg 92, 599–605, doi:10.3171/jns.2000.92.4.0599 (2000). [PubMed: 10761648]
3. Konofagou EE Optimization of the ultrasound-induced blood-brain barrier opening. Theranostics 2, 1223–1237, doi:10.7150/thno.5576 (2012). [PubMed: 23382778]

4. Aryal M, Arvanitis CD, Alexander PM & McDannold N Ultrasound-mediated blood-brain barrier disruption for targeted drug delivery in the central nervous system. Adv Drug Deliv Rev 72, 94–109, doi:10.1016/j.addr.2014.01.008 (2014). [PubMed: 24462453]
5. Sheikov N, McDannold N, Vykhodtseva N, Jolesz F & Hynynen K Cellular mechanisms of the blood-brain barrier opening induced by ultrasound in presence of microbubbles. Ultrasound Med Biol 30, 979–989, doi:10.1016/j.ultrasmedbio.2004.04.010 (2004). [PubMed: 15313330]
6. Tung YS, Vlachos F, Feshitan JA, Borden MA & Konofagou EE The mechanism of interaction between focused ultrasound and microbubbles in blood-brain barrier opening in mice. J Acoust Soc Am 130, 3059–3067, doi:10.1121/1.3646905 (2011). [PubMed: 22087933]
7. Hynynen K, McDannold N, Vykhodtseva N & Jolesz FA Non-invasive opening of BBB by focused ultrasound. Acta Neurochir Suppl 86, 555–558 (2003). [PubMed: 14753505]
8. Windisch M We can treat Alzheimer's disease successfully in mice but not in men: failure in translation? A perspective. Neurodegener Dis 13, 147–150, doi:10.1159/000357568 (2014). [PubMed: 24401335]
9. Snellman A et al. Longitudinal amyloid imaging in mouse brain with 11C-PIB: comparison of APP23, Tg2576, and APPswe-PS1dE9 mouse models of Alzheimer disease. J Nucl Med 54, 1434–1441, doi:10.2967/jnumed.112.110163 (2013). [PubMed: 23833271]
10. Dong J, Revilla-Sanchez R, Moss S & Haydon PG Multiphoton in vivo imaging of amyloid in animal models of Alzheimer's disease. Neuropharmacology 59, 268–275, doi:10.1016/j.neuropharm.2010.04.007 (2010). [PubMed: 20398680]
11. Wang X et al. Noninvasive laser-induced photoacoustic tomography for structural and functional in vivo imaging of the brain. Nat Biotechnol 21, 803–806, doi:10.1038/nbt839 (2003). [PubMed: 12808463]
12. Wang X, Xie X, Ku G, Wang LV & Stoica G Noninvasive imaging of hemoglobin concentration and oxygenation in the rat brain using high-resolution photoacoustic tomography. J Biomed Opt 11, 024015, doi:10.1117/1.2192804 (2006). [PubMed: 16674205]
13. Xu M & Wang LV Photoacoustic imaging in biomedicine. Review of Scientific Instruments 77, 041101, doi:10.1063/1.2195024 (2006).
14. Wang PH et al. Gold-nanorod contrast-enhanced photoacoustic micro-imaging of focused-ultrasound induced blood-brain-barrier opening in a rat model. J Biomed Opt 17, 061222, doi:10.1117/1.JBO.17.6.061222 (2012). [PubMed: 22734752]
15. Kneipp M et al. Effects of the murine skull in optoacoustic brain microscopy. J Biophotonics 9, 117–123, doi:10.1002/jbio.201400152 (2016). [PubMed: 25919801]
16. McDannold N, Vykhodtseva N & Hynynen K Use of ultrasound pulses combined with Definity for targeted blood-brain barrier disruption: a feasibility study. Ultrasound Med Biol 33, 584–590, doi:10.1016/j.ultrasmedbio.2006.10.004 (2007). [PubMed: 17337109]
17. Prahl SA Optical properties spectra compiled by Scott Prahl, < http://omlc.ogi.edu/spectra/> (1999).
18. Kim S, Chen YS, Luke GP & Emelianov SY In vivo three-dimensional spectroscopic photoacoustic imaging for monitoring nanoparticle delivery. Biomed Opt Express 2, 25402550, doi:10.1364/BOE.2.002540 (2011).
19. Li M-L et al. Simultaneous molecular and hypoxia imaging of brain tumors in vivo using spectroscopic photoacoustic tomography. Proceedings of the IEEE 96, 481–489 (2008).
20. Alzheimer's A 2015 Alzheimer's disease facts and figures. Alzheimers Dement 11, 332–384 (2015). [PubMed: 25984581]
21. Lahiri DK et al. A critical analysis of new molecular targets and strategies for drug developments in Alzheimer's disease. Curr Drug Targets 4, 97–112 (2003). [PubMed: 12558063]
22. Tarasoff-Conway JM et al. Clearance systems in the brain-implications for Alzheimer disease. Nat Rev Neurol 11, 457–470, doi:10.1038/nrneurol.2015.119 (2015). [PubMed: 26195256]
23. Luke GP, Yeager D & Emelianov SY Biomedical applications of photoacoustic imaging with exogenous contrast agents. Ann Biomed Eng 40, 422–437, doi:10.1007/s10439-011-04494 (2012). [PubMed: 22048668]

24. Hu S, Maslov K, Tsytsarev V & Wang LV Functional transcranial brain imaging by optical-resolution photoacoustic microscopy. J Biomed Opt 14, 040503, doi:10.1117/1.3194136 (2009). [PubMed: 19725708]

25. Lythgoe MF, Sibson NR & Harris NG Neuroimaging of animal models of brain disease. British Medical Bulletin 65, 235–257, doi:10.1093/bmb/65.1.235 (2003). [PubMed: 12697629]

26. Sehlin D et al. Antibody-based PET imaging of amyloid beta in mouse models of Alzheimer's disease. Nat Commun 7, 10759, doi:10.1038/ncomms10759 (2016). [PubMed: 26892305]

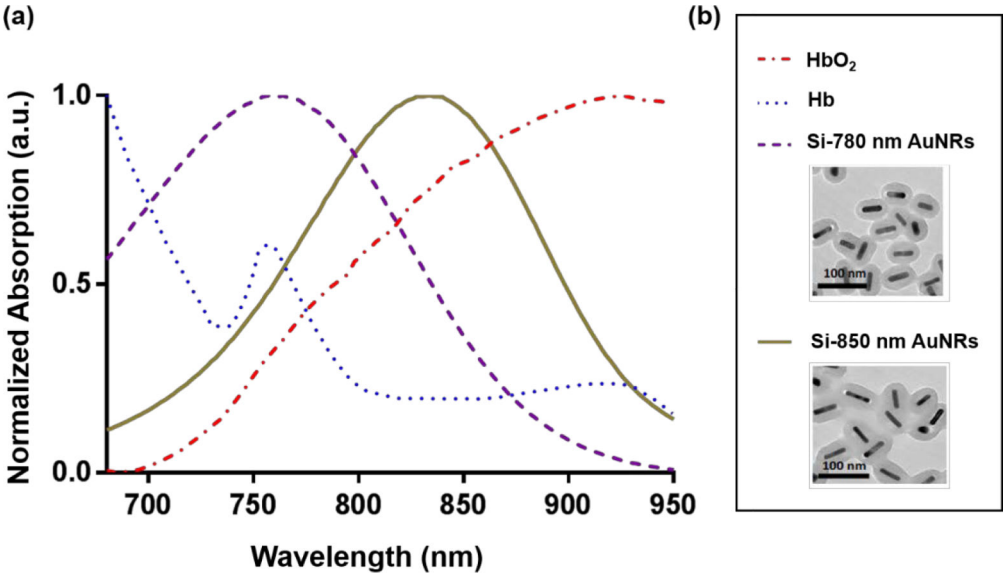

Figure 1:

Contrast agent spectra for USPA imaging (a) Absorption spectra of gold nanorods (AuNRs) and blood measured using UV-VIS spectroscopy and reported in literature, respectively[17]. Spectra include Si-AuNRs with peak absorption wavelengths of 780 nm and 850 nm and endogenous contrast, oxygenated and deoxygenated blood. (b) Spectra key and TEM images of Si-AuNRs obtained from Nanohybrids, Inc.

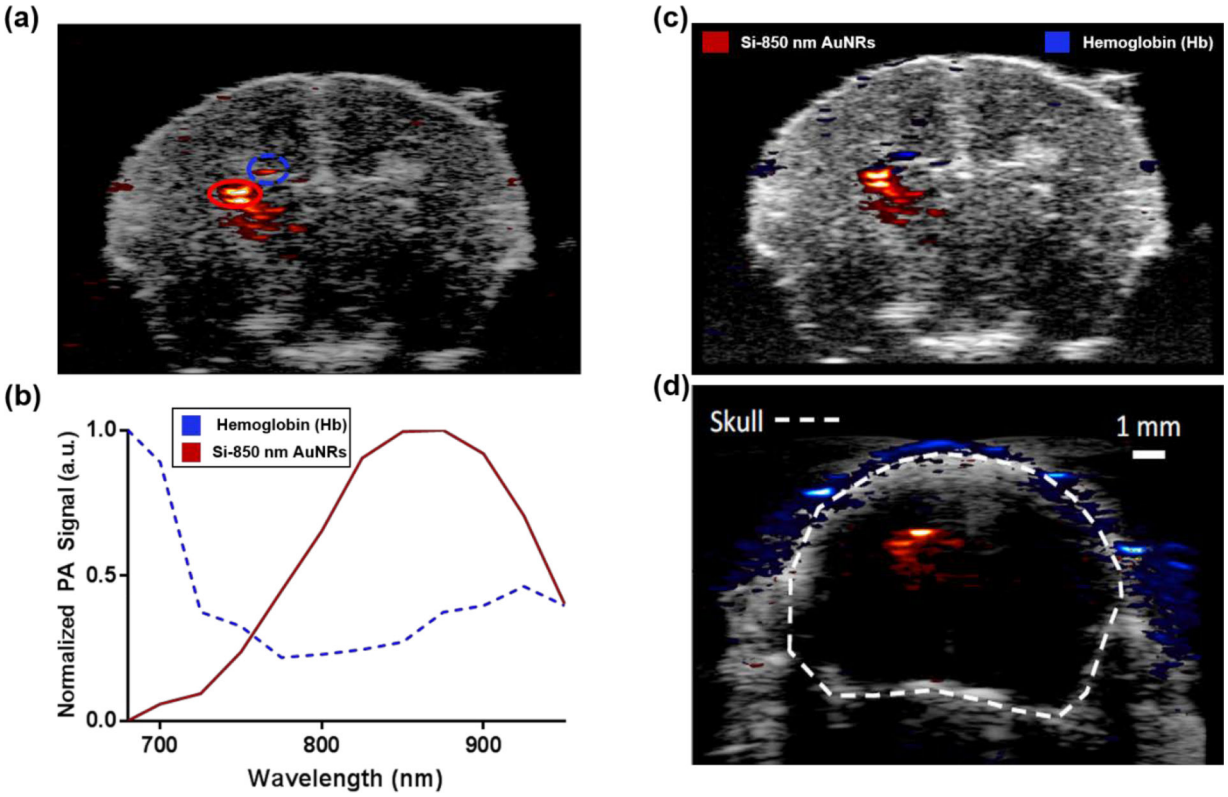

Figure 2:

Ex vivo imaging of murine brain with AuNRs delivered locally (a) USPA image of the coronal plane of the brain *ex vivo*. Here PA signal intensity at 850 nm wavelength is overlaid on top of the grayscale US image. (b) Normalized PA signal captured from the red and blue regions marked on pane A. Normalized PA signal is plotted at each imaging wavelength and assigned as deoxyhemoglobin or Si-850 AuNR based on the ratiometric analysis performed. (c) Processed USPA image of excised brain, distinguishing Si-850 nm AuNR pixels (red) from deoxyhemoglobin pixels (blue). (d) Processed USPA image of excised brain with skull intact, distinguishing Si-850 nm AuNR pixels from deoxyhemoglobin pixels. With an intact skull, the hemoglobin signal at the location of AuNR delivery is minimized.

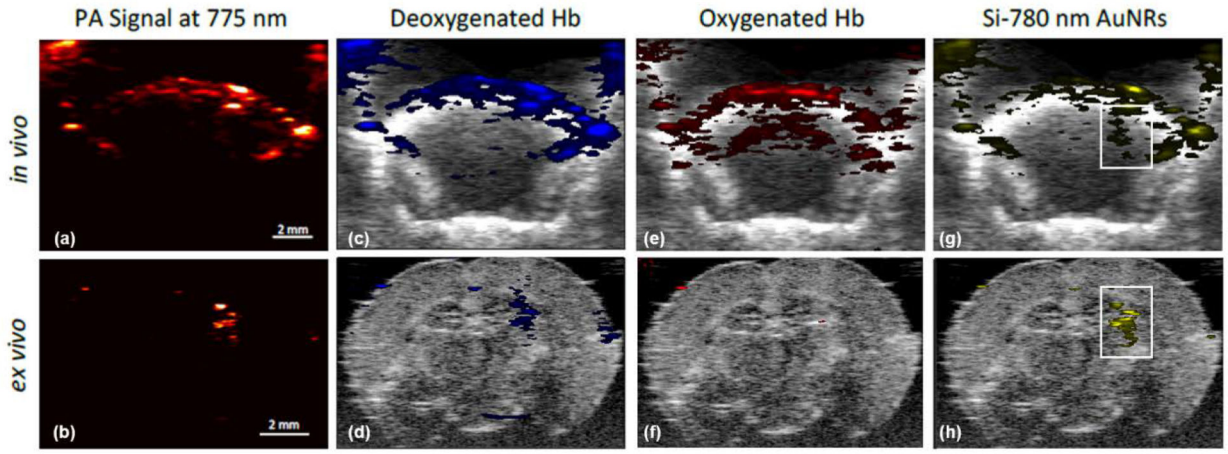

Figure 3:

In vivo and *ex vivo* USPA imaging of locally delivered silica coated gold nanorods (Si-AuNRs) (a)–(b) Unprocessed PA signal of *in viv*o imaging and *ex vivo* excised brain imaging (c)–(h) *In vivo* and *ex vivo* images spectrally unmixed for deoxygenated hemoglobin (c)–(d), oxygenated hemoglobin 2(e)–(f), and Si-AuNRs with 780 nm peak optical absorption (g)–(h). White outlines indicate delivery of AuNRs to the right side of the brain, where FUS BBB opening was applied and occurred.

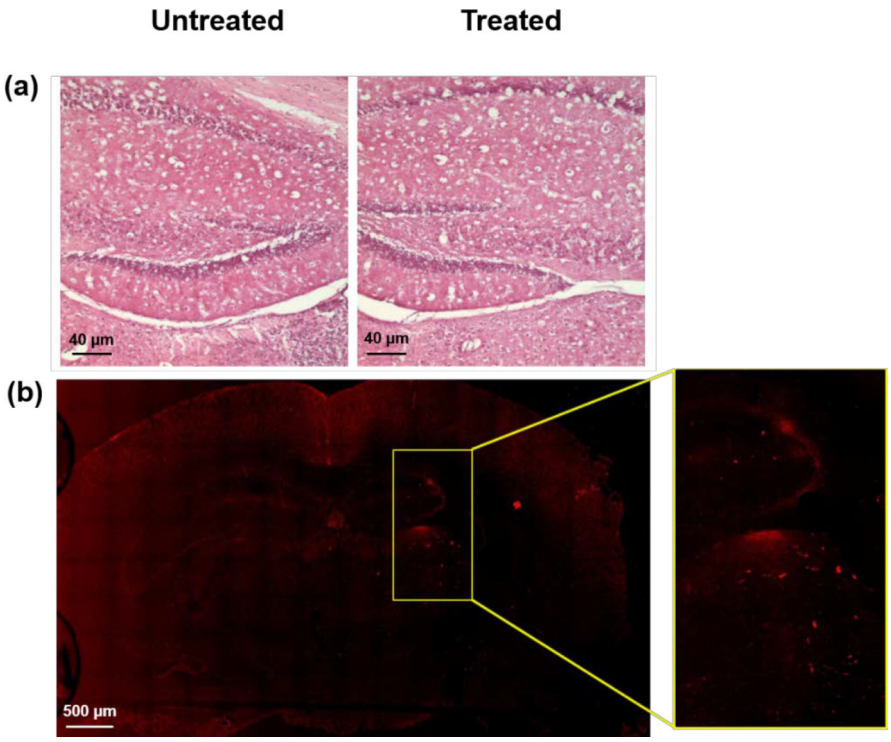

Figure 4:
Histological analysis of brain tissue 4(a) H&E staining of the untreated (left) and treated (right) sides of the brain 4(b) Two photon microscopy showing AuNR signal on the right (treated) side of the brain.